Cell, Vol. 99, 485–497, November 24, 1999, Copyright ©1999 by Cell Press

Shroom, a PDZ Domain–Containing Actin-Binding Protein, Is Required for Neural Tube Morphogenesis in Mice

Jeffrey D. Hildebrand and Philippe Soriano*
Program in Developmental Biology and
Division of Basic Sciences
Fred Hutchinson Cancer Research Center
1100 Fairview Avenue North
Seattle, Washington 98109-1024

Summary

Using gene trap mutagenesis, we have identified a mutation in mice that causes exencephaly, acrania, facial clefting, and spina bifida, all of which can be attributed to failed neural tube closure. This mutation is designated *shroom* (*shrm*) because the neural folds "mushroom" outward and do not converge at the dorsal midline. *shrm* encodes a PDZ domain protein that is involved at several levels in regulating aspects of cytoarchitecture. First, endogenous Shrm localizes to adherens junctions and the cytoskeleton. Second, ectopically expressed Shrm alters the subcellular distribution of F-actin. Third, Shrm directly binds F-actin. Finally, cytoskeletal polarity within the neuroepithelium is perturbed in mutant embryos. In concert, these observations suggest that Shrm is a critical determinant of the cellular architecture required for proper neurulation.

Introduction

Neural tube closure is accomplished by a complex morphogenetic program requiring precisely choreographed cellular proliferation, differentiation, adhesion, and migration (Schoenwolf and Smith, 1990). The sensitivity of neurulation to even slight alterations in this developmental program probably accounts for the observation that neural tube defects (NTDs) affect nearly one in every thousand human births (Copp et al., 1990; Golden and Chernoff, 1995). Neurulation proceeds in a series of steps by which the neural plate is shaped, elongated, and bent to form a tube that extends the entire length of the anterior–posterior (AP) axis. To form the neural tube, the neural plate undergoes a bending process by which the lateral edges, or neural folds, elevate, rotate around the actin-rich dorsal–lateral hinge points (DLHPs), and converge at the dorsal midline (Smith and Schoenwolf, 1997). Following convergence, the edges fuse to form a seamless tube. In the cranial region, closure is initiated at defined fusion points located at the anteriormost point of the forebrain, the forebrain/midbrain boundary, and the hindbrain/spinal chord boundary (Sakai, 1989). Following fusion, closure along the remainder of the neural tube proceeds in a zipper-like fashion in defined directions. Rostral NTDs are typically manifest as exencephaly, acrania, and craniofacial clefting, while caudal NTDs can result in spina bifida.

A number of intrinsic and extrinsic genetic, molecular, and environmental factors that regulate neural tube morphogenesis in mice have been identified. For example, targeted mutations in the genes for *twist* and *cart1* demonstrate a critical role for the surrounding head mesenchyme in neurulation (Chen and Behringer, 1995; Zhao et al., 1996). In contrast, NTDs caused by targeted mutations in the *jnk*, *p300*, *ski*, and *hes1* genes are due to intrinsic defects in the proliferation, survival, and differentiation of neuroepithelial cells (Ishibashi et al., 1995; Berk et al., 1997; Yao et al., 1998; Kuan et al., 1999).

While these examples provide insights into some of the factors that determine neurulation, they provide limited information regarding the identity and regulation of the intrinsic structural molecules that facilitate the conversion of the neural plate into the neural tube. This extensive remodeling necessitates coordinated changes in cell shape, adhesion, and migration, and both pharmacological and genetic approaches have uncovered a clear role for the cytoskeleton in this process. For example, treatment of embryos with cytoskeletal disrupting agents blocks neural tube closure (Karfunkel, 1971; Ybot-Gonzalez and Copp, 1999). In support of these pharmacological results, vinculin (Xu et al., 1998a), Marcks (Stumpo et al., 1995), MacMarcks (Chen et al., 1996; Wu et al., 1996), Mena/profilin I (Lanier et al., 1999), and Arg/Abl (Koleske et al., 1998), all of which are either cytoskeletal proteins or putative regulators of cytoskeletal dynamics, have been linked to neurulation via the generation of knockout mice. While it remains to be precisely determined how these mutations and treatments elicit such phenotypes, defects in DLHP formation and neural fold convergence are found in each case.

During neurulation cells regulate adhesion between neighboring cells and the underlying basement membrane through the use of specialized cell–cell and cell–extracellular matrix (ECM) adhesion structures. Typically, these interactions are mediated by transmembrane receptors that bind ligand on the outside of the cell and are indirectly linked to actin filaments by intricate protein complexes on the inside of the cell (Gumbiner and McCrea, 1993; Burridge and Chrzanowska-Wodnicka, 1996). In addition, these complexes also initiate signals that regulate gene expression, cell proliferation, and differentiation (Gumbiner, 1996; Parsons, 1996). Perhaps the best-characterized cell–cell adhesion structure is the adherens junction (AJ). In these structures, receptors of the cadherin superfamily mediate homotypic intercellular interactions with their large extracellular domains, while their cytoplasmic tails are linked to the actin cytoskeleton via catenins, α-actinin, and vinculin (Menkel et al., 1994; Rimm et al., 1995; Weiss et al., 1998). This interaction with F-actin nucleates the formation of a dense, submembranous actin belt that serves to link adjacent cells and regulate cell shape, migration, and polarity (Gumbiner, 1996). Unfortunately, the exact role of AJs in neurulation has not been established because the molecules that form these structures are required

*To whom correspondence should be addressed (e-mail: psoriano@fhcrc.org).

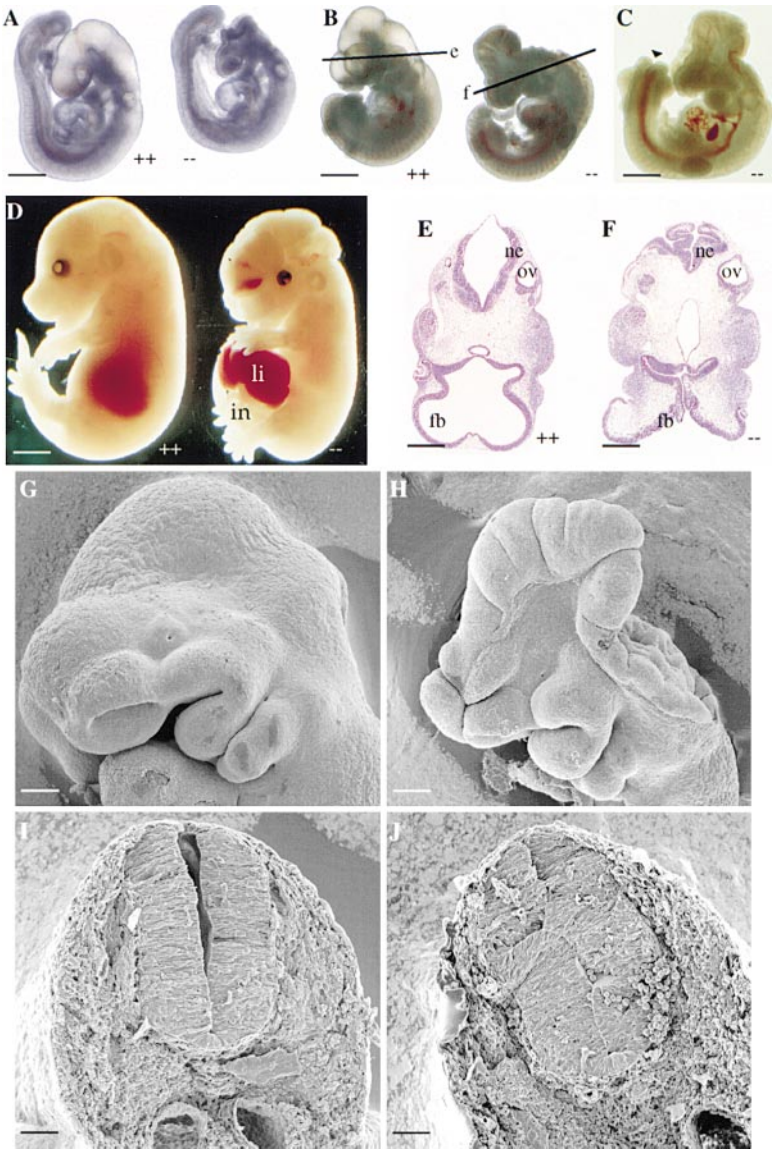

Figure 1. Phenotype of *shrm* Mutant Embryos

(A–D) *shrm* mutant embryos isolated at E9.5 (A), E10.25 (B and C), and E14.5 (D). (A) Lateral view of a wild-type and mutant E9.5 embryo. (B and C) Lateral views of E10.25 wild-type and *shrm* mutant embryos. Lines in (B) denote the positions of the transverse sections in (E) and (F), while the arrowhead in (C) denotes spina bifida. (D) Lateral view of E14.5 wild-type and mutant embryos with herniation of the liver (li) and intestines (in).

(E and F) Transverse, H&E-stained sections of E10.25 wild-type (E) and *shrm* mutant (F) embryos. Note the abnormal morphology of the neural tube (nt) and that the forebrain (fb) neuroepithelium (ne) is not fused.

(G–J) Scanning electron microscopy of E10.25 wild-type (G and I) and *shrm* mutant (H and J) embryos. (G and H) Lateral views of the head. Magnification is 55×. (I and J) Fixed embryos were cut transversely just anterior to the forelimb, mounted on the dorsal side, and viewed. Magnification is 180×. ov, otic vesicle; ++, wild type; - -, homozygote. Bars, 200 μm (A); 250 μm (B and C); 300 μm (D); 100 μm (E–J); 40 μm (I–J).

at earlier stages of development (Larue et al., 1994; Haegel et al., 1995; Torres et al., 1997). While cadherins and catenins are necessary for many normal developmental processes, disruption of AJs also correlates with the oncogenic and metastatic potential of some tumors (Breen et al., 1993; Oyama et al., 1994; Kawanishi et al., 1995).

This report describes the identification and characterization of *shroom* (*shrm*), a mouse mutation that causes exencephaly, acrania, facial clefting, spina bifida, and herniation of internal organs. The *shrm* gene is expressed in the neuroepithelium, the ventrolateral body wall, and the gut, suggesting these phenotypes result directly from a loss of Shrm protein. *shrm* encodes a PDZ domain–containing cytoskeletal protein that can directly bind F-actin and regulate its subcellular distribution in cells. In addition, we show that cytoskeletal polarity is perturbed in Shrm-deficient neuroepithelium. Taken together, these results suggest a cytoskeletal basis for the severe NTDs observed in *shrm* mutant embryos.

Results

Characterization of the *shroom* Mutation

As part of an ongoing analysis of developmental gene trap mutants, we identified a recessive, lethal gene trap mutation, ROSA-53, that causes extensive NTDs. In light of the observation that the neural folds "mushroom" away from the dorsal midline, this mutation has been designated *shroom* (*shrm*).

To characterize the *shrm* phenotype, mutant embryos from embryonic day (E) 8.25 to E17.5 were isolated and analyzed. Most *shrm* embryos are viable at all embryonic stages, indicating that *shrm* mutants survive to term but probably died during or very shortly after birth. Mutant embryos can be distinguished phenotypically by E9.25, as the lateral edges of the cranial neural folds are wavy in appearance and have not converged at the dorsal midline (Figure 1A). By E10.25 the phenotype is manifest as an open neural tube that extends rostrally from the otic vesicle (Figures 1B–1D and 1H). Occasionally, de-

fects in caudal neural tube closure occur, resulting in spina bifida (Figure 1C, arrowhead). Histological analysis and scanning electron microscopy of transverse sections through E10.25 *shrm* mutant embryos show that the neural tube is malformed along the entire AP axis and the forebrain neuroepithelium is exposed (Figures 1F and 1J). Specifically, the neural tube is foliated, and the roof plate is abnormal. Other midline structures and surrounding tissues, such as the notochord, floor plate, head mesenchyme, and somites, appear normal in *shrm* mutant embryos. By E14.5, failed neural tube closure results in exencephaly, acrania, and facial clefting (Figure 1D). Some *shrm* mutants also display defects in ventral closure, resulting in herniation of the intestine and liver (Figure 1D).

Not all of the observed phenotypes are fully penetrant. While all homozygous mutant embryos exhibited exencephaly, 87% (68/78) of the E11.5–E17.5 mutant embryos exhibited definitive craniofacial clefting, and 23% (21/93) of the E10.5–E17.5 mutant embryos displayed spina bifida. A small number, 8% (21/279), of heterozygous embryos displayed a much less severe form of exencephaly (data not shown). Finally, only 12% (7/59) of the E13.5–E17.5 mutant embryos displayed clear defects in ventral closure. Because only a small percentage of *shrm* mutant embryos exhibit ventral closure defects, the remaining analysis focuses on the fully penetrant neural tube defect.

Expression of *shrm*

The gene trap vector used to generate the *shrm* mutation contains a β-galactosidase reporter gene that should be expressed under the control of the trapped gene's endogenous promoter. Therefore, heterozygous *shrm* embryos were isolated and stained with X-gal to determine the temporal and spatial expression of the reporter. At E8.75, prior to the onset of the phenotype, intense staining is detected in the rostral portion of the embryo in the cranial neuroepithelium (Figures 2A and 2E). In the trunk region at this stage, staining is seen in the neural tube, the paraxial mesoderm, and the gut (Figures 2A, 2E–2G). The robust expression of *shrm* in the neuroepithelium rostral to the otic vesicle, but not in the surrounding head mesenchyme, correlates well with the temporal and spatial onset of the fully penetrant phenotypes and strongly supports the hypothesis that Shrm acts autonomously within the neuroepithelium. At E10.5, expression in the rostral portion of the embryo is localized to the neural tube and forebrain (Figures 2B and 2H). In the trunk region, *shrm* expression is detected in the neural tube, somites, ventral body wall, heart, and gut (Figures 2B, 2H–2J). Interestingly, *shrm* expression in the neural tube is quite dynamic, suggesting that only certain cells or processes require Shrm function during neurulation. Specifically, *shrm* expression is limited to the floor and roof plates as development progresses but appears more widespread during the formation of the neural tube (Figure 2H). The strong expression of *shrm* in the ventral body wall and gut is consistent with the ventral closure defects exhibited by some mutant embryos. By E14.5 of development, *shrm* expression is restricted to the skeletal muscle, distal tips of the digits, and forebrain (Figure 2D). The expression pattern determined by X-gal staining has been confirmed by whole-mount RNA in situ hybridization using a probe to the trapped gene (data not shown).

shrm Embryos Are Patterned Correctly

There are several possible mechanisms that could explain the NTDs observed in *shrm* mutant embryos, including abnormalities in patterning that act autonomously within the neuroepithelium. The expression of *shrm* in the cranial neuroepithelium, but not in the head mesenchyme, makes this a particularly realistic model. Conversely, based on the expression of *shrm* in the paraxial mesoderm and the previous report that mesoderm can play a role in patterning the neural tube (Grapin-Botton et al., 1998), it is possible that the caudal NTDs observed in *shrm* mutant embryos are secondary to a defect in paraxial mesoderm. To test these models, wild-type and *shrm* mutant embryos were assayed by whole-mount RNA in situ hybridization or immunostaining to detect alterations in patterning. Probes to *wnt3A* (Figures 3A and 3B), *wnt1*, *krox20*, and *sonic hedgehog* (data not shown) were used to assess patterning of the neural tube and axial mesoderm; probes for *twist* (Figure 3C), *PDGFα receptor* (Figure 3D), and Mox1 protein (Figure 3E) were used to evaluate paraxial mesoderm and head mesenchyme; and an antibody to neurofilament was used to test for neuronal neural crest derivatives (Figure 3F). The only notable difference is in the expression domain of *wnt3A*, which is slightly expanded and diffuse at the dorsal midline of mutant embryos (Figure 3B). However, this expression pattern may be secondary to the abnormal roof plate and undulated nature of the neural tube. In addition, it is well documented that alterations in cranial neural crest cells can cause NTDs. To determine whether the *shrm* phenotype results from a neural crest defect, we assayed the integrity of the cranial skeleton, as many of these structures are derived from neural crest cells (reviewed in Le Douarin et al., 1993). In mutant embryos, the bones comprising the cranial vault do not form, and while the bones that make up the base of the skull are present, they tend to be slightly smaller and less well developed (data not shown). It is likely that these defects are secondary to the exencephalic development of the brain.

NTDs can also result from an imbalance between cell proliferation and cell survival in the neural tube, paraxial mesoderm, and/or head mesenchyme. Therefore, wild-type and mutant E9.75 embryos were assayed to determine the relative amounts of apoptosis (data not shown) and cell proliferation (Figures 3G–3I). These assays reveal no significant differences between wild-type and *shrm* mutant embryos, suggesting the phenotype is not related to aberrant cell proliferation or cell survival. Similarly, by counting the nuclei in each of the tissues assayed, it appears that the total number on cells comprising these compartments is unchanged in *shrm* mutant embryos. In addition, histological analysis also suggested there were no overt abnormalities in the tissues that surround and support the neuroepithelium (Figure 1, data not shown). In order to more carefully evaluate the formation of these tissues, wild-type and *shrm* mutant embryos were viewed at high resolution using scanning electron microscopy (Figures 1I, 1J, 3J, and 3K).

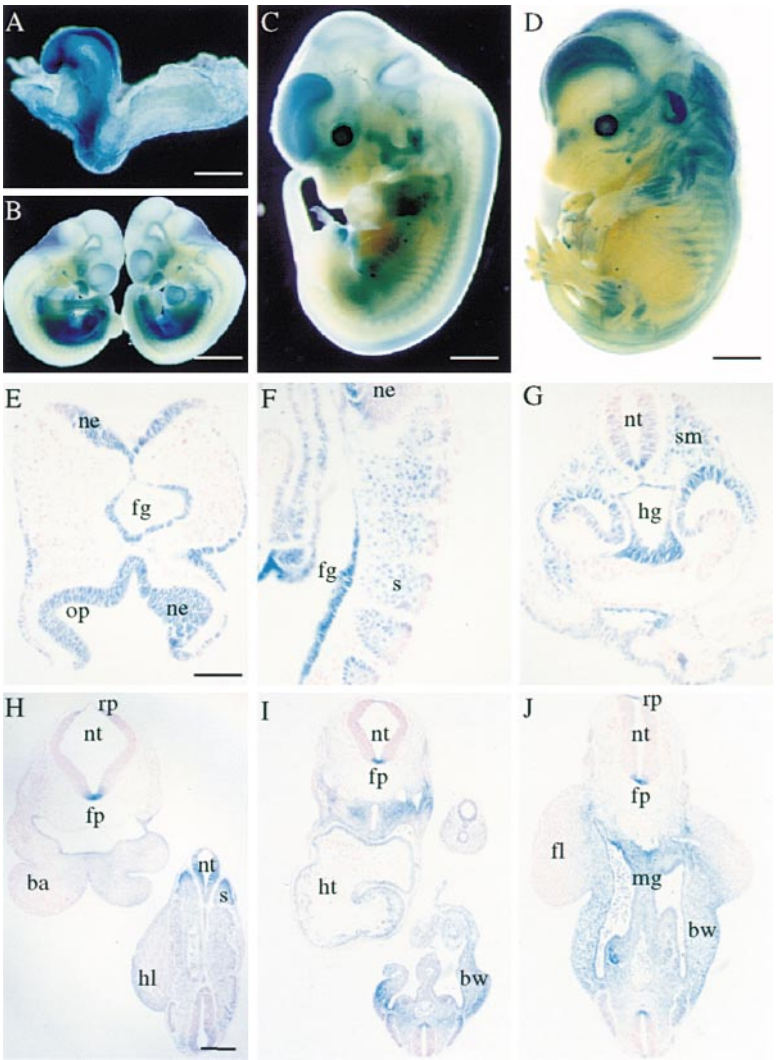

Figure 2. Embryonic Expression of the Gene Trap Reporter

(A–D) Heterozygous embryos were isolated and assayed by whole-mount X-gal staining to determine the temporal and spatial expression of the β-gal gene trap reporter at E8.5 (A), E10.5 (B), E12.5 (C), and E14.5 (D) of development.

(E–J) Sections of X-gal-stained *shrm* heterozygous embryos. Transverse (E and G) and sagital (F) sections of E8.5 stained embryos reveal expression in the cranial neuroepithelium (ne), neural tube (nt), optic pits (op), foregut (fg), hindgut (hg), somites (s), and presomitic mesoderm (sm). Note the high level of expression in the cranial neural folds but the absence of expression in the head mesenchyme at this stage. (H–J) Transverse sections through an X-gal-stained E10.5 heterozygous embryo reveal expression in the neural tube (nt), roofplate (rp), floorplate (fp), somitic mesoderm (sm), heart (h), ventral body wall (bw), and midgut (mg). ba, branchial arch; fl, forelimb bud; hl, hindlimb bud. Bars, 100 μm (A); 150 μm (B); 200 μm (C); 300 μm (D); 100 μm (E–J).

Despite the fact that the neural tube is severely malformed, imaging at this resolution reveals no differences in the size, shape, or architecture of the tissues surrounding the neural tube.

In concert, these data suggest there are no alterations in patterning, proliferation, or cell survival affecting either the neuroepithelium, head mesenchyme, or paraxial mesoderm that could account for the observed NTDs. In light of this information, it is possible the NTDs are caused by a structural or mechanical defect that acts autonomously within the cells comprising the neural tube. This is supported by the observation that *shrm* is exclusively expressed in the cranial neural folds, but not in the surrounding head mesenchyme, and this tissue is affected in 100% of the mutant embryos observed. Furthermore, as *shrm* is expressed in the caudal neuroepithelium, the mechanism that causes the cranial defects may also cause the caudal defects.

shrm Encodes a Novel PDZ Domain Protein

The cDNA for the trapped gene was cloned using 5′-RACE and library screening. Sequence analysis indicates there are at least two *shrm* transcripts that encode two different putative protein products (Figures 4A and 4B). The longest predicted transcript, *shrmL*, encodes a protein of 1986 amino acids, while the second transcript, *shrmS*, encodes a protein of 1808 amino acids that lacks the N-terminal 177 amino acids of ShrmL. Based on the observation that the 5′RACE product was identical to the 5′ UTR of the *shrmS* transcript, we predict the gene trap insertion occurred 3′ of the translational start site for ShrmL, but 5′ of the translational start site for ShrmS (Figure 4A). Therefore, the observed X-gal staining may represent the expression of *shrmS*. However, RNA in situ hybridization indicates that most cells may normally express both ShrmS and ShrmL (data not shown).

Analysis of the protein sequence indicates that *shrm* belongs to a gene family consisting of *shrm*, *apx*, and *APXL* (Figures 4B–4E). Apx, which appears to be a component or regulator of amilioride-sensitive sodium channels, was identified by expression cloning using an antibody that recognized the apical surface of *Xenopus* epithelial cells (Staub et al., 1992). *APXL* is a human gene named for its similarity to *apx* (Schiaffino et al., 1995). Shrm is 35% and 28% identical to APXL and Apx over the entire length of the protein. ShrmL and APXL

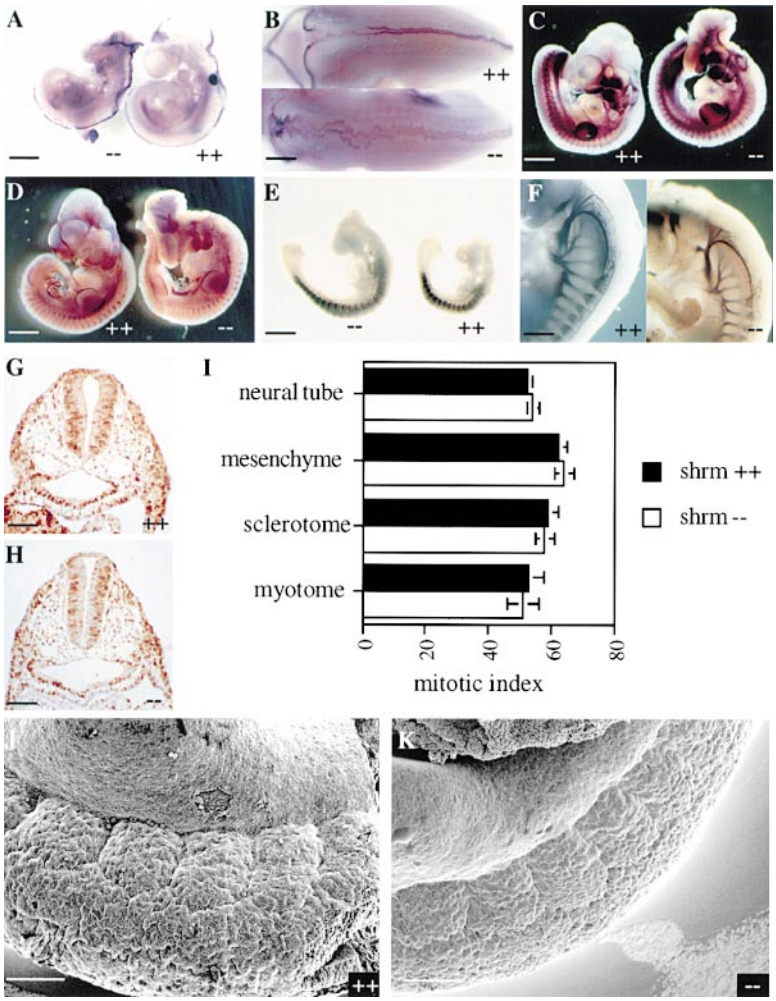

Figure 3. Patterning and Proliferation of *shrm* Mutant Embryos

Wild-type and *shrm* mutant embryos were isolated and assayed by whole-mount RNA in situ hybridization (A–D), whole-mount immunohistochemistry (E and F), BrdU incorporation (G–I), or scanning electron microscopy (J and K).

(A and B) Detection of *wnt3a* at E9.75 ([A], lateral view) or E11.5 ([B], dorsal view).

(C) Lateral view of E10.5 wild-type and *shrm* mutant embryos stained to detect *twist*.

(D) Lateral view of E10.5 wild-type and *shrm* mutant embryos stained to detect *PDGFα receptor*.

(E) Lateral view of E9.25 wild-type and *shrm* mutant embryos stained to detect Mox1.

(F) Lateral view of E10.5 wild-type and *shrm* mutant embryos stained to detect neurofilament.

(G and H) Transverse sections of BrdU-labeled wild-type (G) and mutant (H) E9.75 embryos. Brown nuclei are BrdU-positive cells and indicate active cell proliferation. Sections were counterstained with hematoxylin to detect all nuclei.

(I) Mitotic index in various tissues from wild-type and *shrm* mutant E9.75 embryos. The mitotic index was calculated by dividing the number of BrdU-positive nuclei by the total number of nuclei in each tissue. Data were determined by counting five adjacent sections from two different embryos of each genotype indicated.

(J and K) Lateral view scanning electron micrographs of the somites at the level of the hindlimb in E10.25 wild-type (J) and mutant (K) embryos. Magnification, 150×. Bar, 100 μm.

are 45% identical over the N-terminal 268 amino acids. Within these sequences of Shrm and APXL are single PSD-95/Dgl/ZO-1 (PDZ) domains that are 64% identical. The PDZ domains of ShrmL and APXL are most similar to those found in the Enigma and Ril type Lim domain proteins (Figure 4C; Kuroda et al., 1996). Apx, APXL, and Shrm all contain centrally and C-terminally located domains that are well conserved (Figures 4D and 4E). These domains, ASD1 and ASD2 (*A*px/*S*hrm *d*omain), share no homology with other known proteins and have no identified function. Shrm and APXL are 52% and 60% identical in ASD1 and ASD2, respectively, while Shrm and Apx are 35% and 45% identical in ASD1 and ASD2. Finally, Shrm contains two peptide motifs that might be important for its function: (1) a putative PDZ domain–binding site at its C terminus consisting of the sequence Ser-Pro-Leu (Figure 4E; Songyang et al., 1997) and (2) a consensus binding site for EVH1 domains starting at amino acid 1533 and consisting of the sequence DFPPPPP (Gertler et al., 1996; Niebuhr et al., 1997).

shrm Protein Expression and Subcellular Localization

To biochemically characterize Shrm protein and verify that the trapped allele was protein null, polyclonal antibodies to the C terminus were generated and used for immunoprecipitation and Western blot analysis (Figure 5A). In these experiments, anti-ShrmC antibodies, but not preimmune antibodies, detect proteins of the predicted molecular weights for ShrmS and ShrmL in wild-type embryo lysates (lane 1 versus lane 3). Importantly, expression of these proteins is not detected in *shrm* mutant embryos (lane 2). Similar results were obtained using antibodies to the PDZ domain and Northern blot analysis using nucleotides 632–2534 as a probe detects no *shrm* mRNA in mutant embryos (data not shown). Thus, we predict this mutation causes a null allele for *shrmL* and *shrmS*.

In an effort to understand the cell biological role of *shrm*, we employed indirect immunofluorescence to analyze the subcellular distribution of endogenous Shrm protein in both primary cells derived from wild-type neural tubes (Figure 5B) and neuroepithelial cells cultured in the presence of FGF-2 (Kilpatrick and Bartlett, 1993; data not shown). In both populations of cells, Shrm localizes to structures that resemble AJs (arrows) and actin stress fibers (arrowheads). To verify these observations, primary neural tube cells were costained to detect Shrm (Figures 5C, 5E, and 5G) and either vinculin (Figure 5D), β-catenin (Figure 5F), or F-actin (Figure 5H). These experiments reveal colocalization of Shrm with vinculin

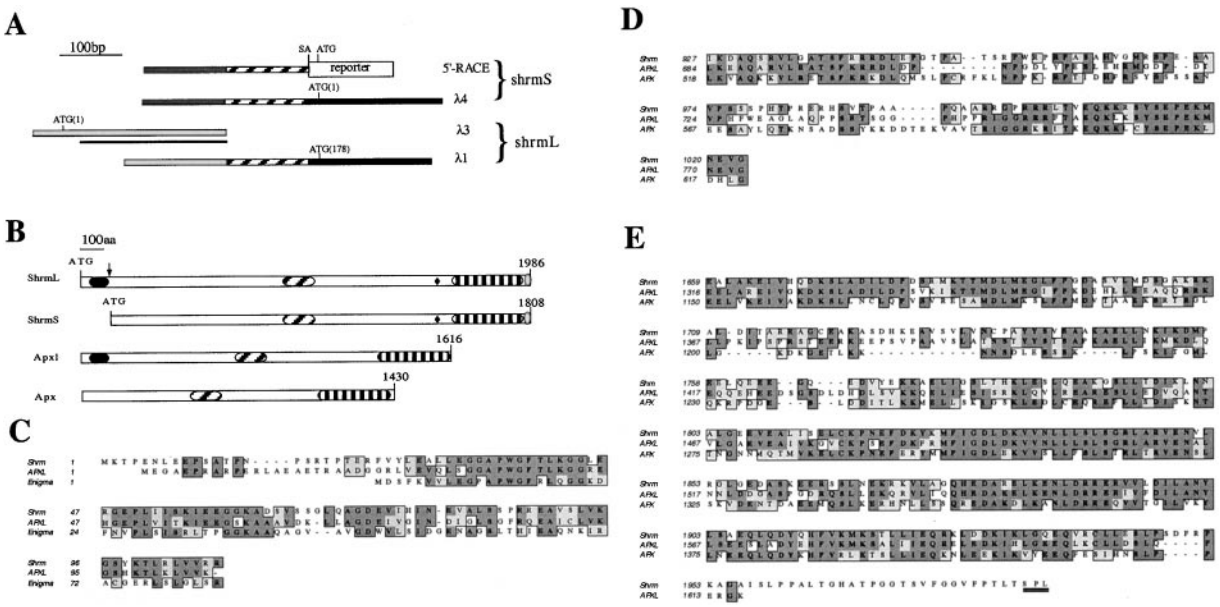

Figure 4. Cloning of *shrm*

(A) Schematic representation of the 5′ ends of *shrmL* and *shrmS* transcripts. cDNAs encoding the remainder of the protein are not depicted. SA, splice acceptor; reporter, βgalCre; underlined portion encodes the PDZ domain; dark gray region, *shrmS*-specific exon of 5′ UTR; hatched and black regions, exons common to *shrmL* and *shrmS* transcripts; light gray regions, *shrmL*-specific sequences for the 5′UTR and PDZ domain.

(B) Schematic of ShrmL and ShrmS in relation to the predicted structures of APXL and Apx. Vertical arrow, site of the gene trap insertion; black oval, PDZ domain; hatched oval, ASD1; striped oval, ASD2; diamond, putative EVH1-binding site; light gray oval, PDZ domain–binding site.

(C) Sequence alignment of the PDZ domains from Shrm, APXL, and Enigma.

(D and E) Sequence alignments of ASD1 and ASD2, respectively. Identical or conserved amino acids are boxed in dark gray or light gray, respectively. Underlined amino acids in (E) constitute the putative PDZ domain–binding site.

and β-catenin in AJs. Note that Shrm does not colocalize with vinculin in focal adhesions, sites of cell–ECM contact (Figure 5D, double arrowhead). This analysis also shows that Shrm colocalizes with F-actin in both stress fibers and AJs. Similar analysis of cells derived from mutant embryos reveals no Shrm staining in AJs or stress fibers. However, these cells possess vinculin- and β-catenin-positive AJs and adhere to fibronectin, laminin, and collagen, suggesting that Shrm is not absolutely required for the formation of cell–cell or cell–ECM adhesion structures (data not shown).

Shrm Can Direct the Subcellular Distribution of Actin

To address the possibility that Shrm could regulate aspects of cytoskeletal architecture, we assayed the consequences of overexpressing ShrmL in mouse epithelial cells (MLP-29 cells) that normally express low levels of Shrm protein (data not shown). In these experiments, a population of transfected cells exhibit abnormal actin structures that are partially coincident with the ectopically expressed protein (Figures 6A–6C). These structures appear to be actin aggregates that are surrounded by ShrmL. To begin defining the domain structure of Shrm, various portions of Shrm were expressed in MLP-29 cells and assayed for the ability to induce the aggregation of F-actin. Actin aggregates are efficiently induced by amino acids 1–1264 (Figures 6D–6F), ShrmS, and amino acids 286–1264, but not by amino acids 1–711 and 1474–1986, indicating that the PDZ and ASD2 domains are not required for this activity (data not shown).

To determine whether the observed actin structures were caused by the ability of Shrm to recruit actin to ectopic sites, a fusion protein between amino acids 1–1264 of Shrm and the membrane-anchoring sequence of the ActA protein of *Listeria monocytogenes* (Shrm1-1264ActA) was expressed in MLP-29 cells. In eukaryotic cells, this sequence of ActA targets proteins to the mitochondrial outer membrane (Bubeck et al., 1997). Following transfection, cells were assayed for the subcellular distribution of Shrm1-1264ActA and F-actin. This fusion protein is efficiently expressed and, based on staining with Mito Tracker, targeted to the mitochondria (Figure 6G, data not shown). Costaining of cells with phalloidin reveals the recruitment of F-actin to mitochondria that display Shrm1-1264ActA on their surface (Figure 6H). It should be noted that both Shrm1-1264ActA and ShrmL do not colocalize exactly with F-actin (Figures 6C and 6I). In these experiments Shrm1-1264ActA causes the aggregation of mitochondria, a result similar to that observed for other actin-binding proteins targeted to mitochondria (Bubeck et al., 1997). Thus, it appears that Shrm can function to direct the subcellular distribution of F-actin in vivo.

Shrm Is an F-Actin-Binding Protein

The above data suggest that Shrm may either induce the polymerization of new actin filaments or recruit existing

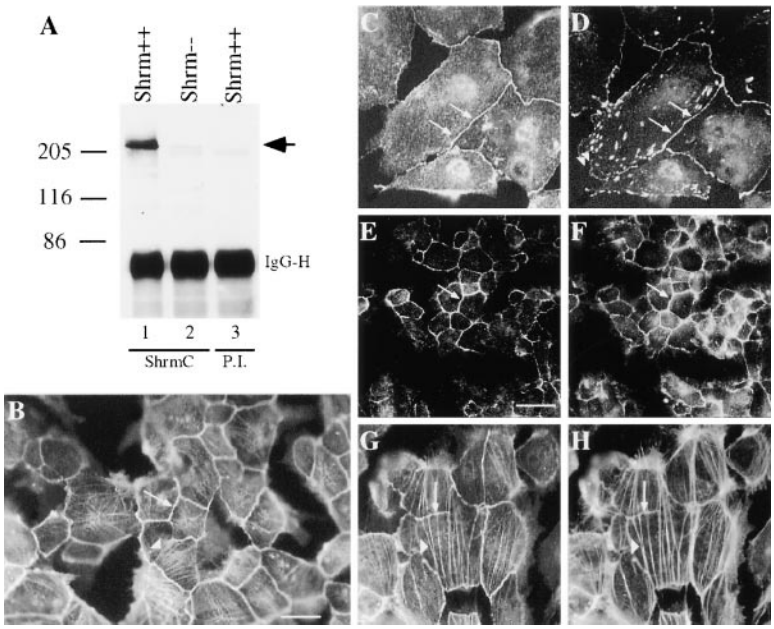

Figure 5. Shrm Protein Expression and Subcellular Localization

(A) Shrm was immunoprecipitated from wild-type (++) and mutant (- -) E12.5 embryo extracts with anti-ShrmC (lanes 1 and 2) or preimmune sera (PI, lane 3) and detected by Western blot using anti-ShrmC. Arrow denotes ShrmS and ShrmL protein.

(B–H) Primary neural tube cells from wild-type embryos were labeled with anti-ShrmC alone (B) or costained to detect Shrm and vinculin ([C] and [D], respectively), Shrm and β-catenin ([E] and [F], respectively), or Shrm and F-actin ([G] and [H], respectively). In (B)–(H), arrows denote AJs, arrowheads indicate actin stress fibers, and the double arrowhead highlights focal adhesions. Bar, 20 μm.

filaments to ectopic sites. To begin addressing these possibilities, we mapped the region of Shrm that targets it to F-actin by expressing fragments of Shrm in RAT1 fibroblasts and assaying them for subcellular localization. In these cells, ShrmL is efficiently targeted to actin stress fibers (Figures 7A–7C). Similarly, a portion of Shrm consisting only of amino acids 754–953 is also targeted to actin stress fibers, albeit somewhat less efficiently than ShrmL (Figure 7D-7F), suggesting the actin targeting sequence is located within these amino acids. Conversely, a protein consisting of amino acids 1474–1986 does not localize to the cytoskeleton and is cytosolic (Figures 7G–7I). While amino acids 754–953 of Shrm contain only a portion of ASD1, suggesting this domain is not required for actin binding, constructs that contain all of ASD1 localize much more efficiently to F-actin. It is known that the PDZ domain of Shrm does not participate in actin localization, as ShrmS is targeted to actin stress fibers and a fragment of Shrm containing amino acids 1–711 is cytosolic (data not shown). To

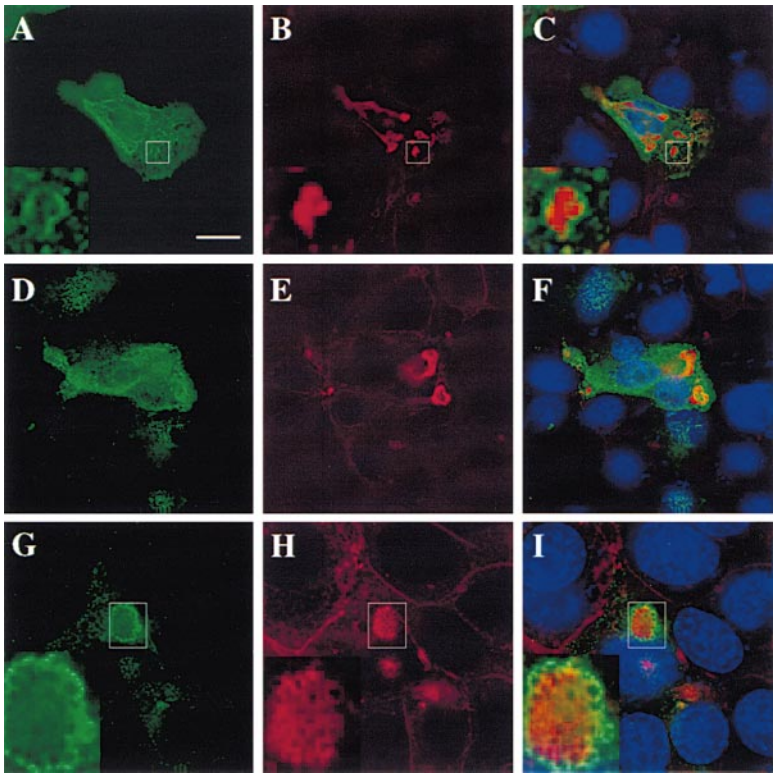

Figure 6. Shrm Recruits Actin to Ectopic Sites

MLP-29 epithelial cells expressing ShrmL (A–C), Shrm1–1264 (D–F), or Shrm1–1264 ActA (G–I) were labeled to detect Shrm (A, D, and G,) and F-actin (B, E, and H); merge (C, F, and I). Boxed regions in (A)–(C) and (G)–(I) are enlarged (insets) to show ShrmL-induced actin aggregates and recruitment of F-actin to mitochondria by Shrm1–1264ActA. Bar, 20 μm.

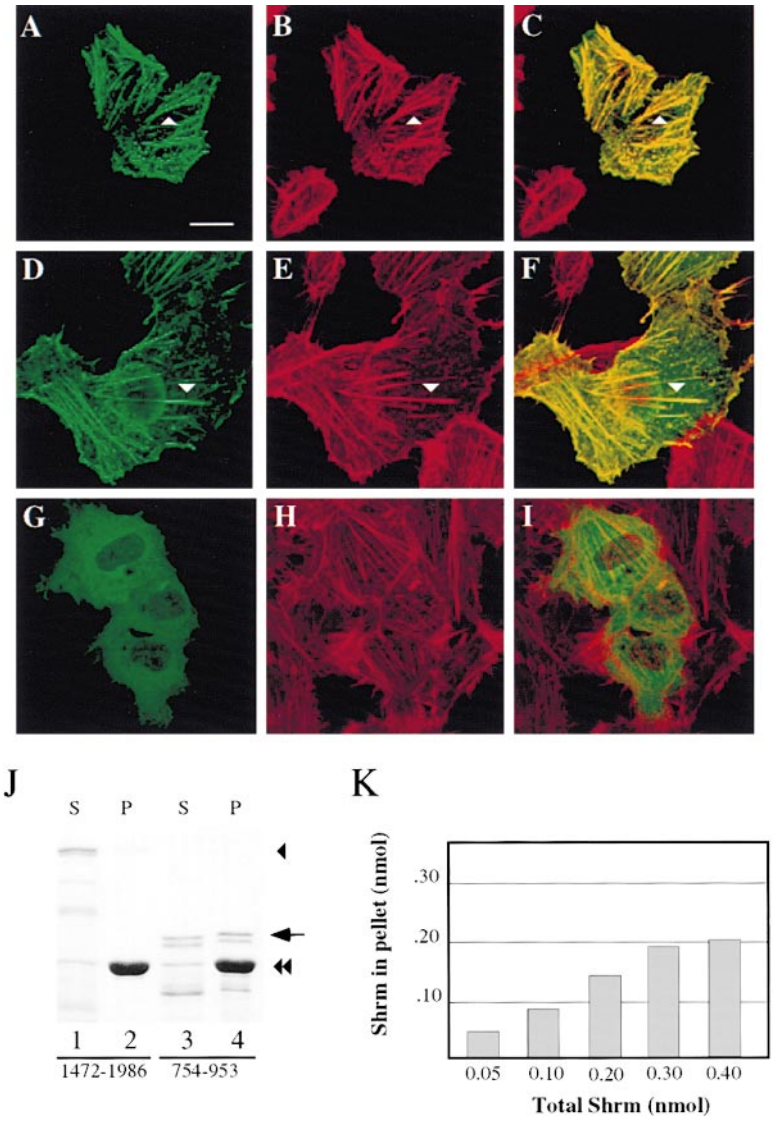

Figure 7. Shrm Is an Actin-Binding Protein

(A–H) RAT1 fibroblasts expressing ShrmL (A–C), Shrm754–953 (D–F), and Shrm1474–1986 (G–H) were labeled to detect Shrm (A, D, G) and F-actin (B, E, H); merge (C, F, I). Arrowhead shows colocalization. Bar, 20 μm. (J and K) The interaction of Shrm with F-actin was assayed in vitro using a cosedimentation assay. Coomassie blue–stained gels of supernatant (s) and pellet (p) fractions resulting from sedimentation of solutions containing F-actin plus either GST754–953 (lanes 3 and 4) or GST1474–1986 (lanes 1 and 2). Quantification of the interaction between GST754–953 and F-actin is shown in (K). Arrow, GST754–953; arrowhead, GST1474–1986; double arrowhead, actin.

determine whether Shrm localization is due to a direct interaction with F-actin, we assayed a GST fusion protein containing amino acids 754–953 of Shrm for the ability to bind F-actin in a cosedimentation experiment (Figure 7J). In these experiments, GST754–953 is found in the pellet, indicating it can directly bind F-actin (Figure 7, lane 4, arrow). Conversely, a GST fusion protein containing amino acids 1474–1986 of Shrm is found only in the supernatant fraction and not in the F-actin pellet (Figure 7J, lanes 1 and 2, arrowhead). No fusion protein is precipitated in the absence of F-actin (data not shown). Initial analysis to determine the kinetics of this interaction suggests the binding is saturable (Figure 7K). These results, in conjunction with those in the previous section, suggest that Shrm is an F-actin-binding protein that can recruit existing actin filaments to ectopic sites in the cell.

Shrm as a Determinant of Cytoskeletal Polarity

The above results suggested a cytoskeletal basis for the NTDs exhibited by *shrm* mutant embryos. To address this hypothesis, we assayed the subcellular distribution of F-actin, β-catenin, and cortactin in the neuroepithelium of wild-type and mutant E9.75 embryos. In wild-type embryos, β-catenin (Figure 8A) and F-actin (Figure 8A′) are colocalized (Figure 8A′′) at the apical surface of the neuroepithelium. In *shrm* mutant embryos, however, β-catenin and F-actin are poorly localized to the apical surface and are more diffuse (Figures 8B-8B′′). Likewise, the apical localization of cortactin, a cortical actin-binding protein, is also significantly reduced in *shrm* mutant embryos (Figures 8D and 8F) as compared with wild-type embryos (Figure 8C and 8E). Costaining of these sections with DAPI to localize nuclei did not reveal significant alterations in the overall apical–basal polarity of these cells, indicating that the observed defects may affect only specific aspects of cellular organization.

To further determine whether the *shrm* phenotype is due to an autonomous defect in the cytoskeletal polarity of the neuroepithelium, the cranial neural folds from E8.75–E9.0 (12–15 somites) wild-type and mutant em-

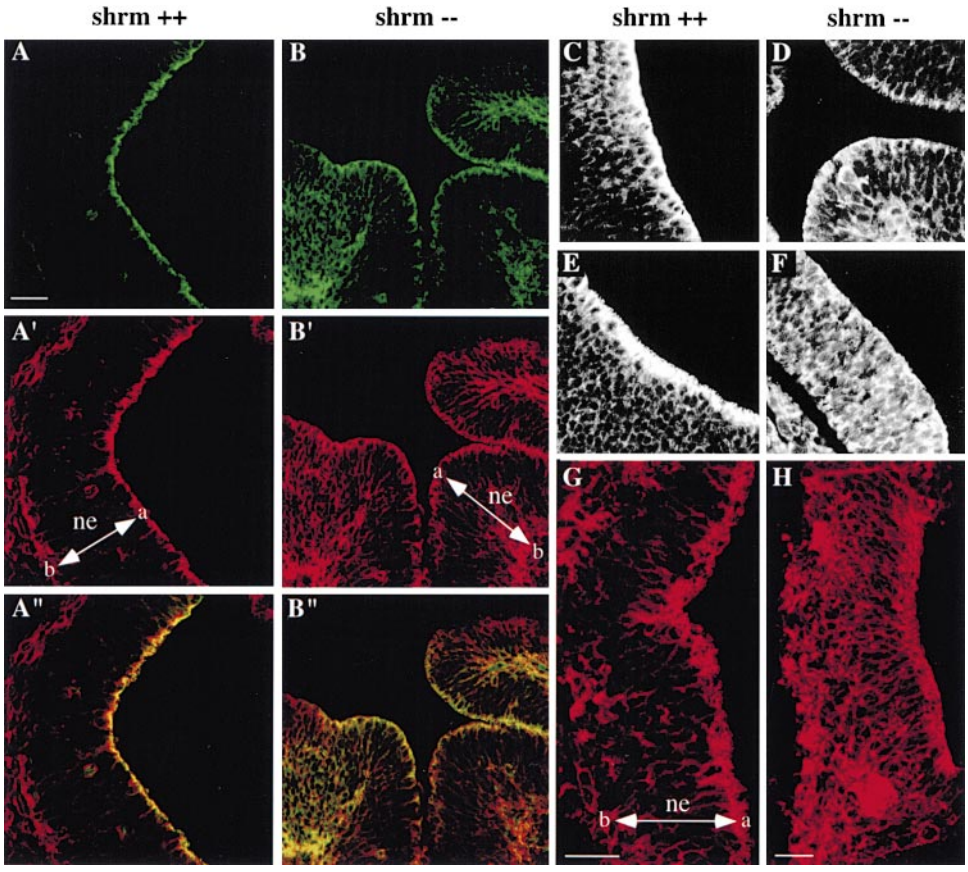

Figure 8. Abnormal Cytoskeletal Architecture in *shrm* Neural Tubes

(A and B) Frozen sections of wild-type (A) or *shrm* mutant (B) E9.75 embryos were assayed by fluorescent immunohistochemistry to detect the localization of β-catenin (A and B) and F-actin (A′ and B′); merge (A′′ and B′′). Sections are from the region of the otic vesicle.

(C–F) Paraffin sections from E9.75 wild-type ([C] and [E], hindbrain and forebrain, respectively) or *shrm* mutant ([D] and [F], hindbrain and forebrain, respectively) embryos were subjected to fluorescent immunohistochemistry to detect the distribution of cortactin.

(G and H) Subcellular distribution of actin in frozen sections of neuroepithelium isolated from wild-type (G) and mutant (H) embryos at the 12–15 somite stage of development and grown in collagen gels. In mutant samples, substantially less actin is found associated with the apical surface. It should be noted that the cytoskeletal architecture in wild-type samples is slightly perturbed due to in vitro culture.

The double-headed arrow denotes the apical (a)–basal (b) polarity of the neuroepithelium (ne). Bar, 50 μm.

bryos were dissected away from the surface ectoderm and surrounding mesenchyme and grown in collagen gels. At this stage, mutant and wild-type embryos are phenotypically indistinguishable, and there were no obvious differences between mutant and wild-type tissues following in vitro culture (data not shown). After 36 hr of growth in vitro, the tissues were sectioned and stained with phalloidin to determine the status of the actin cytoskeleton. In wild-type samples, actin is predominantly localized to the apical surface, indicating the overall cytoskeletal polarity of the neural epithelium is maintained in culture (Figure 8G). Due to atypical development in culture, the apical localization of actin in the wild-type cultures is slightly perturbed relative to that observed in vivo. In mutant samples grown in culture, however, the subcellular distribution of F-actin is significantly shifted away from the apical surface, similar to what is seen in *shrm* mutant embryos in vivo (Figure 8H). Together, these data indicate that Shrm is involved in cytoskeletal architecture and its activity is a critical intrinsic factor of neural tube closure.

Discussion

This report describes the identification and characterization of a recessive lethal mouse mutation designated *shrm*. The primary defect exhibited by *shrm* mutant embryos is a pronounced failure in proper neural tube morphogenesis. Several lines of evidence suggest that *shrm* acts autonomously within the neuroepithelium to facilitate neurulation at the level of cellular cytoarchitecture. First, *shrm* is strongly expressed in the rostral neuroepithelium at the time of cranial neural tube closure and is not expressed in the surrounding head mesenchyme. Importantly, this region of the neural tube is affected in 100% of the *shrm* mutant embryos examined. It is interesting that *shrm* expression within the neuroepithelium is quite dynamic, suggesting that the activity of Shrm may be required for only some aspects of neural tube closure or in specific cell types within the neuroepithelium. At E8.75–E9.25 *shrm* is expressed uniformly in the neural tube rostral to the otic vesicle, while expression is restricted to the floor and roof plates of the neural

tube caudal to the otic vesicle. The expression of *shrm* in the roof plate is interesting, as this is the site where fusion of the neural folds occurs and *shrm* mutant embryos display defects in this process. Second, in contrast to many of the existing mouse mutants that exhibit abnormal neurulation, the *shrm* mutation does not affect patterning or growth in either the neuroepithelium or the surrounding tissues. Third, we show that Shrm is a cytoskeletal protein that can directly bind F-actin and control its subcellular distribution. Finally, in *shrm* mutant embryos, cells comprising the neuroepithelium display clear cytoskeletal defects.

Shrm: A PDZ Domain–Containing Adaptor Protein?

The *shrm* gene encodes a PDZ domain protein, related to Apx and APXL. While nothing is known about the function of APXL, Apx was shown to encode a protein that regulates aspects of sodium channel activity in a manner that is controlled by the actin cytoskeleton (Staub et al., 1992; Prat et al., 1996). By comparing the deduced amino acid sequences of Shrm, Apx, and APXL, we predict that Shrm has a modular nature that would allow it to function as an adaptor molecule or a component of protein complexes. The high degree of sequence conservation between Apx, APXL, and Shrm in ASD1 and ASD2 suggests that these domains may carry out important functions, perhaps as binding surfaces or enzymes. This hypothesis is supported by the fact that ASD1 appears to mediate, at least in part, the interaction of Shrm and F-actin. There are, however, some interesting differences between Shrm, Apx, and APXL. First, the reported sequence of Apx does not contain the PDZ domain. Second, Shrm contains a potential PDZ domain–binding site at its C terminus that is not conserved in Apx or APXL (Songyang et al., 1997). Results from two-hybrid screening suggest this sequence is a functional ligand for PDZ domains, and the significance of these interactions is under investigation.

The presence of a PDZ domain in Shrm is compelling, as these domains mediate protein–protein interactions that facilitate the localization of membrane proteins and the assembly of signaling complexes (Ponting et al., 1997). Extensive genetic, biochemical, and cell biological analysis has been performed in order to elucidate the molecular nature of PDZ domains. Typically, PDZ domains accomplish this by binding the sequence Ser/Thr-Xxx-Val/Iso/Leu located at the C terminus of target protein (Ponting et al., 1997; Songyang et al., 1997). For example, the InaD protein uses its five PDZ domains to assemble a signaling complex consisting of a transmembrane photoreceptor, PKC, and PLC (Tsunoda et al., 1997; Xu et al., 1998b). Similarly, experiments employing biochemistry and *C. elegans* genetics showed that the PDZ domain proteins Lin-2, Lin-7, and Lin-10 form a complex that regulates the basolateral localization of the Let-23 receptor tyrosine kinase in polarized epithelial cells (Kaech et al., 1998).

Shrm is a cytoskeletal protein that is capable of binding F-actin in vitro and directing its subcellular distribution in vivo. These observations are interesting in light of fact that the *shrm* phenotype appears to result from a physical defect in neural tube morphogenesis. Based on the modular nature of Shrm, the above models of PDZ domain function, and the known mechanisms of regulating cell shape and adhesion, it is tempting to predict that Shrm is a multifaceted adaptor protein that acts to determine cytoskeletal polarity or architecture. For example, the PDZ domain could bind the cytoplasmic tail of a membrane receptors while the actin-binding region directly interacts with F-actin. This type of interaction could have at least two possible consequences. In one scenario, this interaction may serve to define cytoarchitecture by anchoring actin stress fibers to the plasma membrane. Conversely, Shrm could function to confine the subcellular distribution of membrane receptors by concentrating them at regions where F-actin is already highly localized. Interestingly, if Shrm acts as an adaptor protein, alternative inclusion of the PDZ domain could significantly modulate its function. Finally, the fact that Shrm has a perfect binding site for EVH1 domains suggests that Shrm may play other roles in modulating actin dynamics by recruiting cytoskeletal regulatory proteins such as VASP, Mena, and Evl (Gertler et al., 1996) to specific sites in the cell.

Shrm, the Cytoskeleton, and Neural Tube Defects

Two critical steps in the process of neural tube closure that appear sensitive to alterations in cytoskeletal integrity are formation of the DLHPs and convergence of the neural folds (Smith and Schoenwolf, 1997). These aspects of neurulation are specific to the cranial neural tube, a region that is severely affected in *shrm* mutant embryos. DLHPs are formed, in part, by changes in cell shape, such that rectangular cells become wedge-shaped, being wider at the basal side and narrower at the apical side. It has also been proposed that a contractile actin-myosin cytoskeleton underlying the apical membrane of the neuroepithelium facilitates neural tube closer by functioning as a "purse string" to pull the neural fold toward the dorsal midline. It is intuitive that these cell shape changes and contractile forces require extensive, well-regulated mechanisms for modulating cell adhesion, cell movement, and cellular architecture. However, recent work indicates that actin filaments are required for maintaining the integrity of the nonbending regions of the neural plate and not for DLHP function (Ybot-Gonzalez and Copp, 1999), thus calling into question the true role of the cytoskeleton in cranial neurulation.

With the discovery that Shrm is a PDZ domain–containing actin-binding protein that colocalizes with F-actin and AJs, it is tempting to speculate that the NTDs we observe are directly related to aberrant cytoskeletal architecture, cell polarity, or cell adhesion. Our results support this hypothesis, since the integrity of the apical cytoskeleton is perturbed in the neuroepithelium of *shrm* mutant embryos. It is currently unclear where Shrm sits in the pathway leading from cadherin-mediated adhesion to cytoskeletal organization. It is possible that Shrm acts at the level of AJ formation. This idea is partially supported by the observation that β-catenin is somewhat mislocalized in *shrm* mutant embryos. However, because Shrm-deficient primary neural tube cells form vinculin- and β-catenin-positive AJs in vitro, we cannot rule out the possibility that the observed perturbation in β-catenin localization is secondary to a cytoskeletal

defect. Alternatively, it is possible that Shrm binds actin and helps to localize or stabilize the cortical cytoskeleton. Both of these possibilities are supported by the mislocalization of F-actin and cortactin in *shrm* mutants.

Since the *shrm* mutation affects specific processes of neural tube formation, this should be a useful mutation for studying the role of the cytoskeleton in neural tube formation. Furthermore, because the *shrm*/*apx* family of genes are different from other known components and regulators of the cytoskeleton, these proteins may carry out unique functions or be involved in new molecular pathways not previously implicated in cellular architecture or embryonic morphogenesis.

Experimental Procedures

Gene Trap Vectors and ES Cells

A gene trap cassette, SAβgalCrepA, containing an adenovirus splice acceptor (Friedrich and Soriano, 1991), a bifunctional gene fusion between β-galactosidase (β-gal) and the Cre recombinase, and the MC1 polyadenylation (pA) sequence (Thomas and Capecchi, 1987) was generated. This cassette was cloned into pGen$^-$ (Soriano et al., 1991) to make the retroviral vector ROSA-βgalCre (ROSA, *r*everse *o*rientation splice *a*cceptor). ROSA-βgalCre was introduced into the packaging line GP+E86 as described (Soriano et al., 1991). Virus was harvested and used to infect AK7 ES cells harboring a reporter that selects for Cre activity. ES cells harboring gene trap insertions were used to generate chimeric mice by blastocyst injection, and germline transmission was achieved by mating male chimeric mice to wild-type females.

Cloning of *shrm*

5′-RACE was carried out using RNA from mutant embryos as described (Frohman et al., 1988). The β-gal gene-specific primers (GSP) used were as follows: GSP1, 5′-CCGTGCATCTGCCAGT TTGAGGGGA-3′; GSP2, 5′-CGACGACAGTATCGGCCTCA-3′; and GSP3, 5′-CAGCTTTCCGGCACCGCTTC-3′. The gene nonspecific primers used were as follows: Q_T, 5′-CCAGTGAGCAGAGTGAC GAGGACTCGAGCT CAAGC(T)17-3′; Q_0, 5′-CCAGTGAGCAGAGT GACG-3′; and Q_1, 5′-GAGGACTCGAGCTCAAGC-3′. A 240–base pair (bp) fragment was isolated and used to screen a mouse brain cDNA library (Stratagene, La Jolla, CA). One clone (λ1) was isolated and sequenced. λ1 contained 120 bp of sequence identical to the 5′-RACE product and 380 bp of unique sequence and was used to screen the brain library and an ES cell cDNA library to obtain further 5′ and 3′ sequence. Mice harboring the mutation are genotyped by Southern blot using the 5′RACE product, which identifies a restriction fragment polymorphism caused by the insertion (data not shown). MacVector and ClustalW were used for sequence analysis and alignments.

Antibodies, Western Blotting, and Immunofluorescence

Chicken anti-Shrm antibodies were generated against GST fusion proteins containing amino acids 1–250 (ShrmN) or amino acids 1474–1986 (ShrmC) by Aves Labs. To immunoprecipitate Shrm, affinity-purified anti-ShrmC (1:100) was added to 500 μg total cell lysate in 1 ml of RIPA lysis buffer derived from mutant or wild-type embryos and incubated at 4°C for 1 hr. Shrm immune complexes were collected with rabbit anti-chicken IgY (Jackson Immunoresearch) bound to protein A-Sepharose 4B (Pharmacia) and washed three times with RIPA and twice with TBS at 4°C. Shrm was detected by Western blot with anti-ShrmC (1:500 dilution), HRP-conjugated goat anti-chicken (1:2500, Jackson Immunoresearch), and ECL reagent (Amersham).

Indirect immunofluorescence on cells and sections was performed using affinity-purified anti-ShrmC (1:25 dilution), anti-ShrmN (1:15), vinculin-specific mAb hVin-1 (Sigma), cortactin-specific mAb 4F11 (10 μg/ml, from T. Parsons), rabbit anti-β-catenin (1:400, from J. Brown and R. Moon), and anti-Myc mAb 9E10 (from R. Scheaff and J. Roberts). Nuclei were stained with DAPI (1:10,000 in PBS, Sigma) for 5 min at room temperature. Primary antibodies were detected using FITC-conjugated donkey anti-chicken (Jackson Immunoresearch), Alexa 488-conjugated goat anti-chicken (Molecular Probes), TR- or FITC-conjugated donkey anti-mouse (1:400, Jackson Immunoresearch), and TR-conjugated donkey anti-rabbit (1:400, Jackson Immunoresearch). F-actin was detected with TRITC-conjugated phalloidin (Sigma). Mitochondria were detected using Mito Tracker Green FM (Molecular Probes) per the manufacturer's recommendations. Cells and sections were fixed and stained as described previously (Gertler et al., 1996; Koleske et al., 1998). Images were captured using either a Zeiss Axioplan, Deltavision deconvolution imaging microscope, or a Leica TCS confocal microscope and processed using Adobe Photoshop.

Isolation and Culture of Neural Tubes

Embryos were isolated and treated with a mixture of Dispase/Collagenase (Boehringer Mannheim) at 1 mg/ml in PBS for 15 min at 4°C followed by 7 min at 37°C. Neural tubes were broken up into smaller pieces and plated onto fibronectin-coated coverslips. Neural tubes were cultured for 3–4 days in DMEM/10% fetal bovine serum (FBS). Alternatively, neuroepithelial cells were isolated and grown in DMEM/10% FBS supplemented with 20 ng/ml FGF-2 (Boehringer Mannheim) and 8 μg/ml heparin as described (Kilpatrick and Bartlett, 1993). After 24 hr, cells were replated and grown in the presence of FGF-2. Colonies of cells exhibiting an epithelial morphology were isolated, pooled, expanded, and tested by either X-gal staining or immunofluorescence staining to determine whether they retained *shrm* expression. These cells were then assayed for cytoskeletal architecture, formation of adhesion structures, and adhesion to ECM components.

For in vitro culture of neural tissue, neuroepithelium was dissected away from the majority of the surface ectoderm and mesenchyme following dispase/collagenase digestion for 10 min at 4°C followed by 4 min at 37°C. Isolated neuroepithelium was imbedded in collagen gel (Collaborative Biomedical) and grown in Hams F12 supplemented with N2 supplement (GIBCO–BRL), glutamine, and antibiotics for 36 hr at 37°C.

Histology

For X-gal staining, embryos were fixed and stained as described (Friedrich and Soriano, 1991). Embryos used for histology were fixed in 4% PFA at 4°C, dehydrated in ethanol, cleared in Histoclear (National Diagnostics), and embedded in paraffin. Five-micrometer sections were mounted on TESPA-coated slides, dewaxed, hydrated, and stained with Harris hematoxylin and eosin-Y (H&E). For immunofluorescence, embryos were fixed in 4% PFA at 4°C, dehydrated in ethanol, cleared in xylene, and embedded in paraffin. Four-micrometer sections were dewaxed and hydrated in PBS prior to addition of antibody. Ten-micrometer frozen sections of embryos and collagen gels were prepared as described (Koleske et al., 1998). Scanning electron microscopy was carried out following a previously described technique (Stanisstreet, 1990).

Whole-mount RNA in situ hybridization and immunohistochemistry was performed as described (Hogan et al., 1994) using the following probes: *twist* 3′ UTR (R. Behringer), *wnt3A* (H. Roelink), 800 bp fragment from *krox20* (W. Shawlot), a 2.5 kb fragment of rat *sonic hedgehog* (H. Roelink), the 3′UTR of *PDGFα receptor* (M. Tallquist et al., unpublished data), rabbit anti-Mox1 serum (C. Wright and A. Candia), and anti-neurofilament mAb 2H3 (T. Jessell). TUNEL analysis, to detect apoptosis, and BrdU incorporation, to detect proliferating cells, were performed as described (Soriano, 1997).

Expression of Shrm Variants

The following Shrm constructs were generated and used for expression in eukaryotic cells or bacteria. A cDNA encoding ShrmL (1–1986) was assembled and cloned into the expression vector pCS2. Shrm1–1264 was generated by cloning DNA encoding amino acids 1–1264 into pCS2. Shrm1–1264actA was generated by cloning cDNA encoding amino acids 1–1264 into the vector pSPL61–2 (from J. Wehland). For Shrm754–953 and Shrm1474–1986, cDNA encoding amino acids 754–953 and 1474–1986 were cloned into pCS3mt (a derivative of pCS2 containing a Myc epitope tag) or pGEX3X. For transfection assays, 2×10^5 MLP-29 epithelial cells (from E. Medico) or RAT1 fibroblasts were plated on gelatin-coated coverslips, grown over

night in DMEM/10% calf serum, and transfected with 1 μg plasmid DNA using Lipofectamine (GIBCO–BRL) per the manufacturer's recommendations.

Actin Cosedimentation Assay

GST754–953 and GST1474–1986 fusion proteins were expressed and purified from *E. coli*. Purified, eluted fusion proteins were precleared by high-speed centrifugation, added to F-actin (2 μM final concentration, Cytoskeleton, Inc), and incubated for 1 hr at room temperature. F-actin was pelleted by centrifugation in a Beckman Airfuge for 1 hr at 4°C, and equal amounts of the pellet and supernatant fractions were resolved by SDS–PAGE and stained with Coomassie blue. Stained gels were scanned and quantified using NIH image software.

Acknowledgments

We thank the members of the Soriano, Cooper, and Moens Labs for providing useful advice and discussions; M. Basch and M. Bronner-Fraser for advice on in vitro culture of neural tubes; F. Gertler and B. Howell for critically reading this manuscript; K. Weismann, C. Auger, T. Knight, L. Caldwell, and J. Groombridge for excellent technical assistance; and B. Zambrowicz for the ROSA-βgalCre vector. J. D. H. is a fellow of the Leukemia Society of America. This work was supported by National Institutes of Health grant HD24875 to P. S.

Received June 9, 1999; revised October 27, 1999.

References

Berk, M., Desai, S.Y., Heyman, H.C., and Colmenares, C. (1997). Mice lacking the *ski* proto-oncogene have defects in neurulation, craniofacial patterning, and skeletal muscle development. Genes Dev. *11*, 2029–2039.

Breen, E., Clarke, A., Steele, G.J., and Mercurio, A.M. (1993). Poorly differentiated colon carcinoma cell lines deficient in alpha-catenin expression express high levels of surface E-cadherin but lack Ca(2+)-dependent cell-cell adhesion. Cell Adhes. Commun. *1*, 239–250.

Bubeck, P., Pistor, S., Wehland, J., and Jockusch, B.M. (1997). Ligand recruitment by vinculin domains in transfected cells. J. Cell Sci. *110*, 1361–1371.

Burridge, K., and Chrzanowska-Wodnicka, M. (1996). Focal adhesions, contractility, and signaling. Annu. Rev. Cell. Dev. Biol. *12*, 463–519.

Chen, Z.F., and Behringer, R.R. (1995). *twist* is required in head mesenchyme for cranial neural tube morphogenesis. Genes Dev. *9*, 686–699.

Chen, J., Chang, S., Duncan, S.A., Okano, H.J., Fishell, G., and Aderem, A. (1996). Disruption of the MacMARCKS gene prevents cranial neural tube closure and results in anencephaly. Proc. Natl. Acad. Sci. USA *93*, 6275–6279.

Copp, A.J., Brook, F.A., Estibeiro, J.P., Shum, A.S., and Cockroft, D.L. (1990). The embryonic development of mammalian neural tube defects. Prog. Neurobiol. *35*, 363–403.

Friedrich, G., and Soriano, P. (1991). Promoter traps in embryonic stem cells: a genetic screen to identify and mutate developmental genes in mice. Genes Dev. *5*, 1513–1523.

Frohman, M.A., Dush, M.K., and Martin, G.R. (1988). Rapid production of full-length cDNAs from rare transcripts: amplification using a single gene-specific oligonucleotide primer. Proc. Natl. Acad. Sci. USA *85*, 8998–9002.

Gertler, F.B., Niebuhr, K., Reinhard, M., Wehland, J., and Soriano, P. (1996). Mena, a relative of VASP and Drosophila Enabled, is implicated in the control of microfilament dynamics. Cell *87*, 227–239.

Golden, J.A., and Chernoff, G.F. (1995). Multiple sites of anterior neural tube closure in humans: evidence from anterior neural tube defects (anencephaly). Pediatrics *95*, 506–510.

Grapin-Botton, A., Bonnin, M.A., Sieweke, M., and Le Douarin, N.M. (1998). Defined concentrations of a posteriorizing signal are critical for MafB/Kreisler segmental expression in the hindbrain. Development *125*, 1173–1181.

Gumbiner, B.M. (1996). Cell adhesion: the molecular basis of tissue architecture and morphogenesis. Cell *84*, 345–357.

Gumbiner, B.M., and McCrea, P.D. (1993). Catenins as mediators of the cytoplasmic functions of cadherins. J. Cell Sci. Suppl. *17*, 155–158.

Haegel, H., Larue, L., Ohsugi, M., Fedorov, L., Herrenknecht, K., and Kemler, R. (1995). Lack of beta-catenin affects mouse development at gastrulation. Development *121*, 3529–3537.

Hogan, B., Beddington, R., Costantini, F., and Lacy, E. (1994). Manipulating the Mouse Embryo: A Laboratory Manual (Cold Spring Harbor, NY: Cold Spring Harbor Laboratory).

Ishibashi, M., Ang, S.L., Shiota, K., Nakanishi, S., Kageyama, R., and Guillemot, F. (1995). Targeted disruption of mammalian *hairy* and *Enhancer of split* homolog-1 (*HES-1*) leads to up-regulation of neural helix-loop-helix factors, premature neurogenesis, and severe neural tube defects. Genes Dev. *9*, 3136–3148.

Kaech, S.M., Whitfield, C.W., and Kim, S.K. (1998). The LIN-2/LIN-7/LIN-10 complex mediates basolateral membrane localization of the *C. elegans* EGF receptor LET-23 in vulval epithelial cells. Cell *94*, 761–771.

Karfunkel, P. (1971). The role of microtubules and microfilaments in neurulation in Xenopus. Dev. Biol. *25*, 30–56.

Kawanishi, J., Kato, J., Sasaki, K., Fujii, S., Watanabe, N., and Niitsu, Y. (1995). Loss of E-cadherin-dependent cell-cell adhesion due to mutation of the beta-catenin gene in a human cancer cell line, HSC-39. Mol. Cell. Biol. *15*, 1175–1181.

Kilpatrick, T.J., and Bartlett, P.F. (1993). Cloning and growth of multipotential neural precursors: requirements for proliferation and differentiation. Neuron *10*, 255–265.

Koleske, A.J., Gifford, A.M., Scott, M.L., Nee, M., Bronson, R.T., Miczek, K.A., and Baltimore, D. (1998). Essential roles for the Abl and Arg tyrosine kinases in neurulation. Neuron *21*, 1259–1272.

Kuan, C.Y., Yang, D.D., Samanta Roy, D.R., Davis, R.J., Rakic, P., and Flavell, R.A. (1999). The Jnk1 and Jnk2 protein kinases are required for regional specific apoptosis during early brain development. Neuron *22*, 667–676.

Kuroda, S., Tokunaga, C., Kiyohara, Y., Higuchi, O., Konishi, H., Mizuno, K., Gill, G.N., and Kikkawa, U. (1996). Protein-protein interaction of zinc finger LIM domains with protein kinase C. J. Biol. Chem. *271*, 31029–31032.

Lanier, L.M., Gates, M.A., Witke, W., Menzies, A.S., Wehman, A.M., Macklis, J.D., Kwiatkowski, D., Soriano, P., and Gertler, F.B. (1999). Mena is required for neurulation and commissure formation. Neuron *22*, 313–325.

Larue, L., Ohsugi, M., Hirchenhain, J., and Kemler, R. (1994). E-cadherin null mutant embryos fail to form a trophectoderm epithelium. Proc. Natl. Acad. Sci. USA *91*, 8263–8267.

Le Douarin, N.M., Ziller, C., and Couly, G.F. (1993). Patterning of neural crest derivatives in the avian embryo: in vivo and in vitro studies. Dev. Biol. *159*, 24–49.

Menkel, A.R., Kroemker, M., Bubeck, P., Ronsiek, M., Nikolai, G., and Jockusch, B.M. (1994). Characterization of an F-actin-binding domain in the cytoskeletal protein vinculin. J. Cell Biol. *126*, 1231–1240.

Niebuhr, K., Ebel, F., Frank, R., Reinhard, M., Domann, E., Carl, U.D., Walter, U., Gertler, F.B., Wehland, J., and Chakraborty, T. (1997). A novel proline-rich motif present in ActA of Listeria monocytogenes and cytoskeletal proteins is the ligand for the EVH1 domain, a protein module present in the Ena/VASP family. EMBO J. *16*, 5433–5444.

Oyama, T., Kanai, Y., Ochiai, A., Akimoto, S., Oda, T., Yanagihara, K., Nagafuchi, A., Tsukita, S., Shibamoto, S., Ito, F., et al. (1994). A truncated beta-catenin disrupts the interaction between E-cadherin and alpha-catenin: a cause of loss of intercellular adhesiveness in human cancer cell lines. Cancer Res. *54*, 6282–6287.

Parsons, J.T. (1996). Integrin-mediated signaling: regulation by protein tyrosine kinases and small GTP-binding proteins. Curr. Opin. Cell Biol. *8*, 146–152.

Ponting, C.P., Phillips, C., Davies, K.E., and Blake, D.J. (1997). PDZ

domains: targeting signaling molecules to sub-membranous sites. Bioessays *19*, 469–479.

Prat, A.G., Holtzman, E.J., Brown, D., Cunningham, C.C., Reisin, I.L., Kleyman, T.R., McLaughlin, M., Jackson, G.R., Jr., Lydon, J., and Cantiello, H.F. (1996). Renal epithelial protein (Apx) is an actin cytoskeleton-regulated Na^+ channel. J. Biol. Chem. *271*, 18045–18053.

Rimm, D.L., Koslov, E.R., Kebriaei, P., Cianci, C.D., and Morrow, J.S. (1995). Alpha 1(E)-catenin is an actin-binding and -bundling protein mediating the attachment of F-actin to the membrane adhesion complex. Proc. Natl. Acad. Sci. USA *92*, 8813–8817.

Sakai, Y. (1989). Neurulation in the mouse: manner and timing of neural tube closure. Anat. Rec. *223*, 194–203.

Schiaffino, M.V., Bassi, M.T., Rugarli, E.I., Renieri, A., Galli, L., and Ballabio, A. (1995). Cloning of a human homologue of the Xenopus laevis APX gene from the ocular albinism type 1 critical region. Hum. Mol. Genet. *4*, 373–382.

Schoenwolf, G.C., and Smith, J.L. (1990). Mechanisms of neurulation: traditional viewpoints and recent advances. Development *109*, 243–270.

Smith, J.L., and Schoenwolf, G.C. (1997). Neurulation: coming to closure. Trends Neurosci. *20*, 510–517.

Songyang, Z., Fanning, A.S., Fu, C., Xu, J., Marfatia, S.M., Chishti, A.H., Crompton, A., Chan, A.C., Anderson, J.M., and Cantley, L.C. (1997). Recognition of unique carboxyl-terminal motifs by distinct PDZ domains. Science *275*, 73–77.

Soriano, P. (1997). The PDGF alpha receptor is required for neural crest cell development and for normal patterning of the somites. Development *124*, 2691–2700.

Soriano, P., Friedrich, G., and Lawinger, P. (1991). Promoter interactions in retrovirus vectors introduced into fibroblasts and embryonic stem cells. J. Virol. *65*, 2314–2319.

Stanisstreet, M. (1990). Scanning electron microscopy and morphometry. In Postimplantation Mammalian Embryos: A Practical Approach. A.J. Copp and D.L. Cockroft, D.L., eds. (Oxford: IRL Press).

Staub, O., Verrey, F., Kleyman, T.R., Benos, D.J., Rossier, B.C., and Kraehenbuhl, J.P. (1992). Primary structure of an apical protein from Xenopus laevis that participates in amiloride-sensitive sodium channel activity. J. Cell Biol. *119*, 1497–1506.

Stumpo, D.J., Bock, C.B., Tuttle, J.S., and Blackshear, P.J. (1995). MARCKS deficiency in mice leads to abnormal brain development and perinatal death. Proc. Natl. Acad. Sci. USA *92*, 944–948.

Thomas, K.R., and Capecchi, M.R. (1987). Site-directed mutagenesis by gene targeting in mouse embryo-derived stem cells. Cell *51*, 503–512.

Torres, M., Stoykova, A., Huber, O., Chowdhury, K., Bonaldo, P., Mansouri, A., Butz, S., Kemler, R., and Gruss, P. (1997). An *alpha-E-catenin* gene trap mutation defines its function in preimplantation development. Proc. Natl. Acad. Sci. USA *94*, 901–906.

Tsunoda, S., Sierralta, J., Sun, Y., Bodner, R., Suzuki, E., Becker, A., Socolich, M., and Zuker, C.S. (1997). A multivalent PDZ-domain protein assembles signaling complexes in a G-protein-coupled cascade. Nature *388*, 243–249.

Weiss, E.E., Kroemker, M., Rudiger, A.H., Jockusch, B.M., and Rudiger, M. (1998). Vinculin is part of the cadherin-catenin junctional complex: complex formation between alpha-catenin and vinculin. J. Cell Biol. *141*, 755–764.

Wu, M., Chen, D.F., Sasaoka, T., and Tonegawa, S. (1996). Neural tube defects and abnormal brain development in F52-deficient mice. Proc. Natl. Acad. Sci. USA *93*, 2110–2115.

Xu, W., Baribault, H., and Adamson, E.D. (1998a). Vinculin knockout results in heart and brain defects during embryonic development. Development *125*, 327–337.

Xu, X.Z., Choudhury, A., Li, X., and Montell, C. (1998b). Coordination of an array of signaling proteins through homo- and heteromeric interactions between PDZ domains and target proteins. J. Cell Biol. *142*, 545–555.

Yao, T.P., Oh, S.P., Fuchs, M., Zhou, N.D., Ch'ng, L.E., Newsome, D., Bronson, R.T., Li, E., Livingston, D.M., and Eckner, R. (1998). Gene dosage-dependent embryonic development and proliferation defects in mice lacking the transcriptional integrator p300. Cell *93*, 361–372.

Ybot-Gonzalez, P., and Copp, A.J. (1999). Bending of the neural plate during mouse spinal neurulation is independent of actin microfilaments. Dev. Dyn. *215*, 273–283.

Zhao, Q., Behringer, R.R., and de Crombrugghe, B. (1996). Prenatal folic acid treatment suppresses acrania and meroanencephaly in mice mutant for the *Cart1* homeobox gene. Nat. Genet. *13*, 275–283.

GenBank Accession Numbers

The GenBank accession numbers for the ShrmL and ShrmS sequences are AF199421 and AF199422, respectively.